In Operando Monitoring of the Pore Dynamics in Ordered Mesoporous Electrode Materials by Small Angle X-ray Scattering

Gwi Ok Park,[†,#] Jeongbae Yoon,[†,#] Eunjun Park,[‡] Su Bin Park,[§] Hyunchul Kim,[†] Kyoung Ho Kim,[§] Xing Jin,[§] Tae Joo Shin,[⊥,∞] Hansu Kim,[*,‡] Won-Sub Yoon,[*,†] and Ji Man Kim[*,†,§]

[†]Department of Energy Science, Sungkyunkwan University, Suwon 440-746, Republic of Korea, [‡]Department of Energy Engineering, Hanyang University, Seoul 133-791, Republic of Korea, [§]Department of Chemistry, Sungkyunkwan University, Suwon 440-746, Republic of Korea, and [⊥]Pohang Accelerator Laboratory, Pohang 790-784, Republic of Korea. [#]These authors contributed equally to this work. [∞]Present address: UNIST Central Research Facilities & School of Natural Science, Ulsan National Institute of Science and Technology (UNIST), Ulsan 689-789, Republic of Korea.

ABSTRACT To monitor dynamic volume changes of electrode materials during electrochemical lithium storage and removal process is of utmost importance for developing high performance lithium storage materials. We herein report an *in operando* probing of mesoscopic structural changes in ordered mesoporous electrode materials during cycling with synchrotron-based small angel X-ray scattering (SAXS) technique. *In operando* SAXS studies combined with electrochemical and other physical characterizations straightforwardly show how porous electrode materials underwent volume changes during the whole process of charge and discharge, with respect to their own reaction mechanism with lithium. This comprehensive information on the pore dynamics as well as volume changes of the electrode materials will not only be critical in further understanding of lithium ion storage reaction mechanism of materials, but also enable the innovative design of high performance nanostructured materials for next generation batteries.

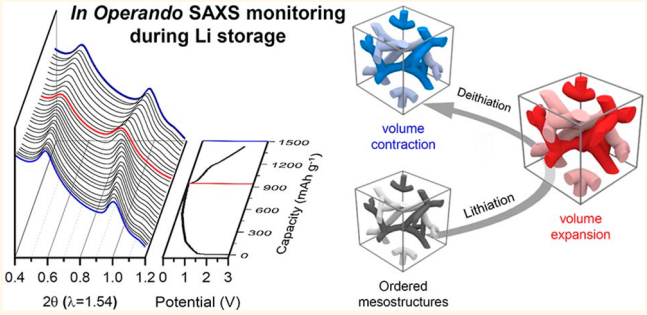

KEYWORDS: mesoporous electrode · *in operando* monitoring · small-angle X-ray scattering · pore dynamics · Li-storage

Lithium ion batteries (LIBs) have attracted much attention as a rechargeable energy-storage system, due to high voltage, long cycle life, low toxicity and high reliability for powering an increasingly diverse range of applications.[1−3] However, the energy density of currently commercialized LIBs is already close to their technological limits. To improve the performance of anode part replacing a currently used graphite (theoretical capacity of 372 mAh g^{-1}), there has been extensive research on developing new anode materials such as metal oxides, silicon- or tin-based metal alloys, and related composite configurations.[1,4−7] As the electrode materials for LIBs, various kinds of nanostructured materials also enable the improvement in the energy density, rate capability and long-term stability because of their high surface area, short distance for mass transport and the increased freedom for volume change during cycling.[3,8,9]

Recently, ordered mesoporous materials have gained much attention as a promising candidate for the electrode materials in LIBs, since the ordered arrays of mesopores and frameworks with uniform sizes in nanometer scale can offer the opportunities to improve the electrochemical performances.[10−14] An advantage of ordered mesoporous materials in LIBs is the existence of well-defined mesopores that is believed to act as a kind of physical buffer for volume changes during the lithiation and delithiation. Therefore, real time monitoring of the mesostructural maintainability of the electrode materials during repeated discharge and charge process is essential in understanding the dynamics of mesoscale pores in the electrode material and proving the importance of mesopores as a buffer

* Address correspondence to khansu@hanyang.ac.kr, wsyoon@skku.edu, jimankim@skku.edu.

Received for review March 4, 2015 and accepted April 13, 2015.

Published online April 13, 2015
10.1021/acsnano.5b01378

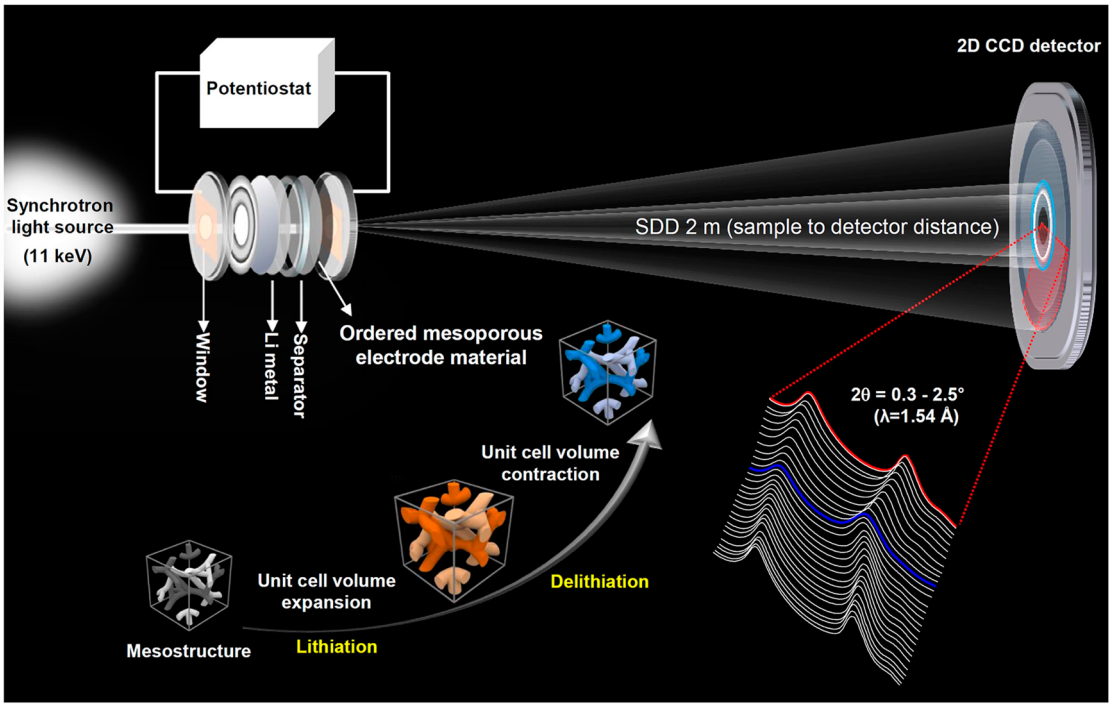

Scheme 1. Schematic illustration for *in operando* small angle X-ray scattering with the coin type *in situ* cell for monitoring of pore dynamics of ordered mesoporous metal oxide electrodes during cycling.

element to sustain huge volume changes and the associated mechanical strains of electrode materials during cycling. Nanostructural changes of the electrode materials can be studied with electron microscopies (EM), especially transmission electron microscopy (TEM).[15−17] However, the application range of these EM-based techniques is limited, because they prove only the local structure and generally do not permit an *in situ* characterization of electrodes. Recently, *in operando* investigation on the electrode materials for lithium ion battery has gained much attention in order to exactly understand the reaction mechanism of the electrode material during cycling. Several reports using soft X-ray absorption and hard X-ray microscopy demonstrated that dynamic variation of the phase transformation and electron and lithium ion dynamics in the electrode material can be obtained, which cannot be monitored with *ex situ* analysis.[18,19] However, the studies on dynamic changes of pores as well as volume changes of the electrode materials could not be found up to date. Small angle X-ray scattering (SAXS) is one of the most useful analytical techniques to investigate properties of porous materials since the SAXS technique works very well in characterizing unique nanostructures of materials with the probing range of 1−100 nm.[20−22] To further gain insights on the nanostructural changes of mesoporous materials during cycling, it is highly required to develop a new analytical technique with *in operando* capability to monitor physical changes of mesopores in the electrode material.

Here, we present a direct monitoring of nanostructural changes in ordered mesoporous electrode materials during the lithium storage process using an *in operando* SAXS technique (Scheme 1). According to our best knowledge, this is the first report for an *in operando* observation of the pore dynamics in the electrode material for LIBs with respect to the degree of lithium storage. In the present work, highly ordered mesoporous titanium dioxide (meso-TiO_2, intercalation reaction), cobalt oxide (meso-Co_3O_4, conversion reaction) and tin oxide (meso-SnO_2, conversion and alloying reaction) were selected to show the significance of the present *in operando* SAXS study. Moreover, we demonstrate that comprehensive SAXS monitoring from *in operando* studies provides direct information for volume changes of ordered mesoporous active material, especially the electrode materials which exhibit the upkeep of mesostructural order during the lithiation and delithiation.

RESULTS AND DISCUSSION

Characterization of Highly Ordered Mesoporous Electrodes. The highly ordered mesoporous electrode materials were prepared by a nanoreplication method from a mesoporous silica template with cubic *Ia*3*d* mesostructure (KIT-6, Supporting Information, XRD pattern, N_2 sorption results and TEM image in Figures S1 and S2). Details on synthesis of highly ordered mesoporous electrode materials are described in the Materials and Methods.[23−26] As shown in the SAXS data for the pristine mesoporous electrode materials (Supporting Information, Figure S3A), all the mesoporous materials exhibit well-defined diffraction patterns in the low-angle region, meaning that the materials possess

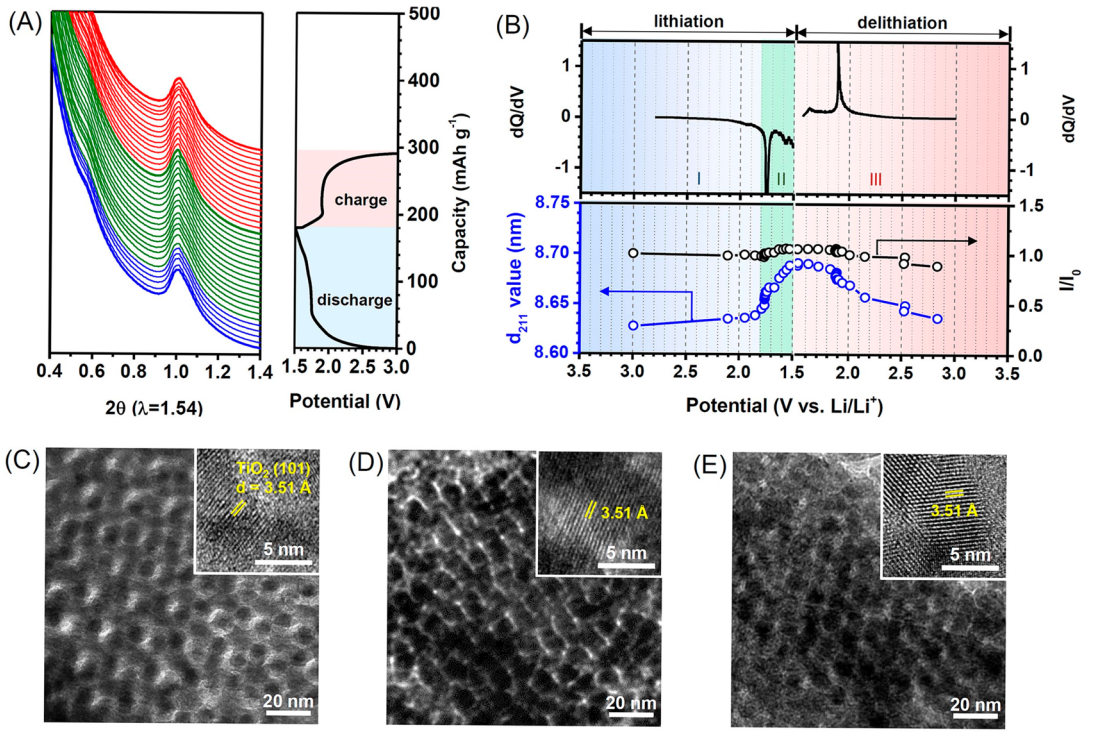

Figure 1. (A) *In operando* SAXS spectra and the corresponding voltage profiles of meso-TiO_2 electrode, (B) differential capacity *vs* potential plot (d*Q*/d*V*), the corresponding changes in lattice parameter and resolved peak intensity ratio calculated from the (211) reflection, and TEM images and HR-TEM images (insets) of (C) pristine, (D) fully lithiated and (E) fully delithiated meso-TiO_2 electrodes.

highly ordered mesostructures. The present mesoporous materials show the similar diffraction patterns with a new peak in the low-angle region after the nanoreplication from the KIT-6 template, which corresponds to the (110) plane. The presence of this (110) peak means the well-known mesostructural transformation during the nanoreplication from the KIT-6 template.[27,28] Wide-angle X-ray diffraction (XRD) patterns (Supporting Information, Figure S3B) indicate that the mesoporous electrode materials are highly crystalline, where the meso-SnO_2 and meso-Co_3O_4 materials exhibit tetragonal rutile phase (JCPDS 41-1445,$P4_2/mnm$) and cubic phase (JCPDS 42-1467, $Fd3m$), respectively. The frameworks of meso-TiO_2 material consist of mainly tetragonal anatase phase (JCPDS 21-1272,$I4_1/amd$) and a quite small portion of rutile phase. The ordered mesostructures with uniform pore sizes and well-defined crystalline frameworks of the mesoporous electrode materials are also confirmed from scanning electron microscopy (SEM) and transmission electron microscopy (TEM) images (Supporting Information, Figure S4). N_2 adsorption–desorption isotherms and the corresponding BJH pore size distribution curves also indicate that the pristine electrode materials exhibit well-developed mesoporosities with high surface areas and large pore volumes (Supporting Information, Figure S5 and Table S1).

***In Operando* SAXS Investigation for Pore Dynamics during Cycling.** To probe dynamic changes of mesoscale pores in the ordered mesoporous electrode materials with respect to the depth of discharge (lithium insertion) and charge (lithium removal), we performed *in operando* SAXS studies using specially designed coin type cell with Kapton window (Scheme 1). *In operando* SAXS data for the meso-TiO_2, meso-Co_3O_4 and meso-SnO_2 electrodes during the first discharge–charge process, thus obtained, are shown in Figures 1A, 2A and 2C, respectively, which clearly indicate the changes of mesoscopic orders depending on their Li-storage mechanisms. We also observed the nanostructural changes in the ordered mesoporous metal oxide electrode before and after cycling using *ex situ* TEM (Figure 1C,D,E and Figure 3).

As shown in Figure 1A, there is no significant change in the *in operando* SAXS data of meso-TiO_2 electrode during the lithiation and delithiation process, which is known to follow the intercalation mechanism of lithium ions.[13,29–31] For more insight, d*Q*/d*V* data, relative SAXS peak intensities and mesoscopic lattice parameters are plotted against the lithiation-delithiation potentials (Figure 1B). The peak intensities are almost same in the potential range of 3–1.5 V, whereas the changes of d_{211} spacing are divided into two regions (I and II) during the lithiation: one is 3–1.75 V that is known to be a solid solution reaction region (only 0.5% increase in mesoscopic cell volume, see Figure 4A) and the other is 1.75–1.5 V for a two phase reaction region (2.2% volume expansion). The d*Q*/d*V* data in Figure 1B also show two well-defined current

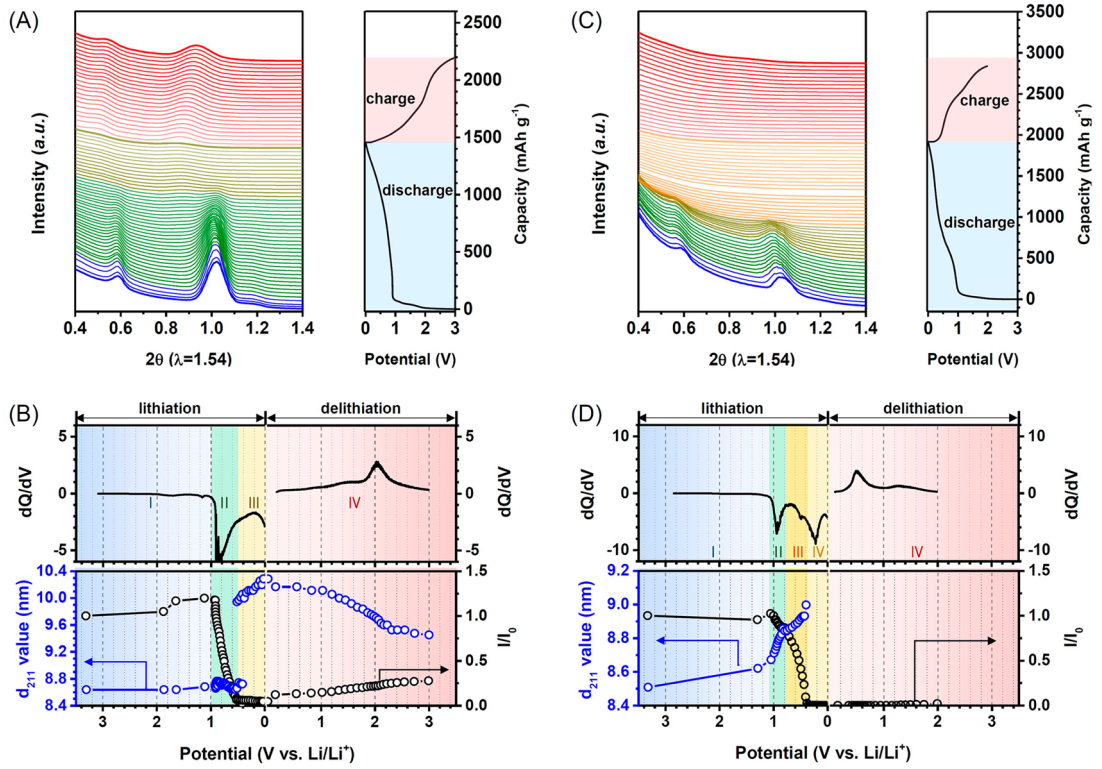

Figure 2. (A) *In operando* SAXS spectra and the corresponding voltage profiles of meso-Co_3O_4, and (B) differential capacity *vs* potential plot (d*Q*/d*V*), and the corresponding changes in lattice parameter and resolved peak intensity ratio from the (211) reflection of meso-Co_3O_4. (C) *In operando* SAXS spectra and the corresponding voltage profiles of meso-SnO_2, and (D) differential capacity *vs* potential plot (d*Q*/d*V*), and the corresponding changes in lattice parameter and resolved peak intensity ratio from the (211) reflection of meso-SnO_2.

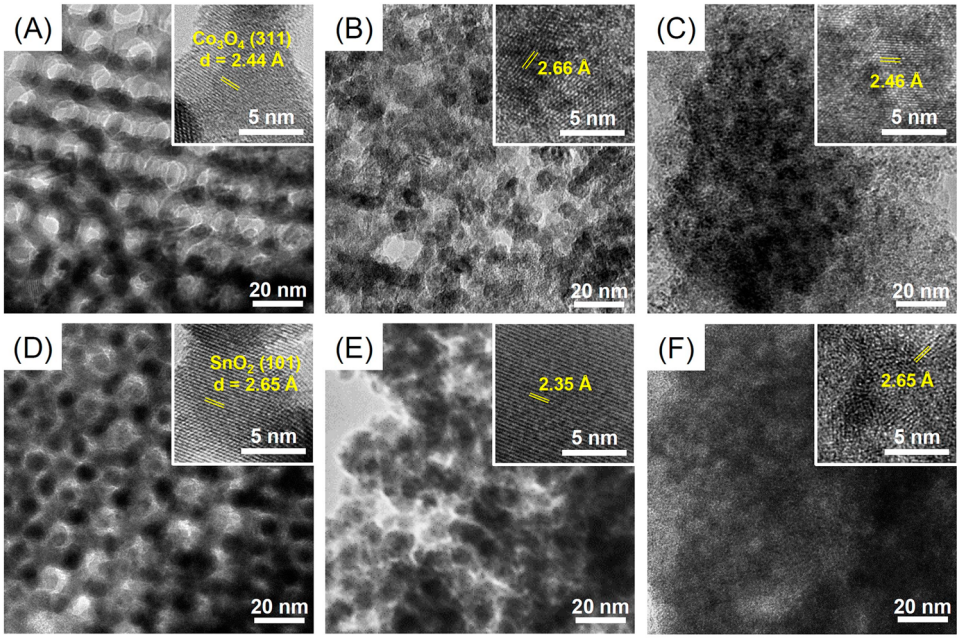

Figure 3. TEM and HR-TEM (insets) images of (A) pristine, (B) fully lithiated and (C) fully delithiated meso-Co_3O_4 electrodes, and (D) pristine, (E) fully lithiated and (F) fully delithiated meso-SnO_2 electrodes.

peaks at 1.75 V during lithiation, which corresponds to the phase transition from tetragonal anatase ($I4_1/amd$) to orthorhombic $Li_{0.54}TiO_2$ (*Imma*). As shown in Figure 4A, the mesoscopic cell volume is recovered to the initial state after complete delithiation (region III in Figure 1B), indicating that the volume changes of the meso-TiO_2 are almost reversible during the discharge–charge process. TEM images and high-resolution TEM

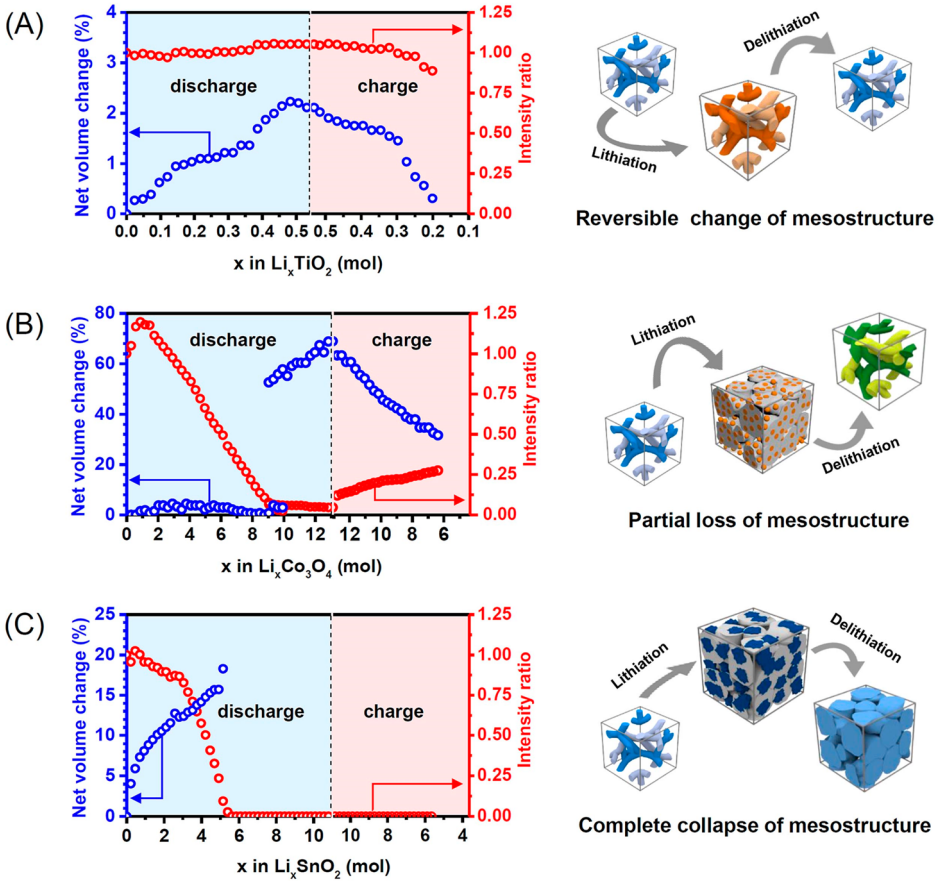

Figure 4. Schematic illustration of pore dynamics in the ordered mesoporous metal oxide electrodes with respect to Li^+ storage reaction mechanism, and net volume change and intensity ratio with contained lithium in the electrode materials for the initial lithiation-delithiation of (A) meso-TiO_2, (B) meso-Co_3O_4, and (C) meso-SnO_2. The net volume change was calculated by using d_{211} spacing of the *in operando* SAXS data of Figure 1 and 2, assuming the mesostructure as the *Ia*3*d* cubic symmetry.

(HR-TEM) images in Figure 1C–E represent the microstructures of pristine, lithiated and delithiated meso-TiO_2 electrodes, respectively, which show that the ordered mesostructure as well as the framework crystallinities are maintained even after lithiation and delithiation.

Figure 2A shows the nanostructural changes of the meso-Co_3O_4 electrode depending on the degree of lithiation, which follows the conversion reaction ($Co_3O_4 + 8\ Li \rightarrow 4\ Li_2O + 3\ Co$, theoretical capacity of 890 mAh g^{-1}).[1,32,33] There are no significant changes of SAXS in the region I of Figure 2B (3–1.0 V, about 0.8 mol of Li are inserted into 1 mol of Co_3O_4). The region II (1.0–0.5 V, 9.9 mol of lithium react with 1 mol of Co_3O_4) represents a rapid decrease in SAXS intensity, indicating the loss of mesostructure upon the conversion reaction to form Co and Li_2O. However, to our surprise, the d_{211} value and the mesoscopic cell volumes in the region II (Figure 2B and Figure 4B) are very similar to those of pristine meso-Co_3O_4 electrode, even though 9.9 mol of lithium per 1 mol of Co_3O_4 are stored which should lead an increase in Co_3O_4 framework volume. This is a direct evidence for the buffer role of mesoporous void volume that can successfully accommodate volume changes of active material upon conversion reaction with lithium. At the potential of 0.5 V, the peak intensity at d_{211} spacing of about 8.7 nm becomes nearly zero, and a new broad SAXS peak appears at the lower angle (around 10 nm). Further lithiation (region III, 0.5–0 V) gives a discharge capacity of 1456 mAh g^{-1} (13.1 mol of Li) and 70% mesoscopic cell volume expansion. During the delithiation step (region IV), the intensity of SAXS peak increases again, but the mesoscopic cell volume and the peak intensity do not resile from the pristine electrodes (Figure 2B and Figure 4B). This irreversible mesostructural change is probably due to a well-known delithiation reaction ($Co + Li_2O \rightarrow CoO + 2\ Li^+ + 2e^-$).[1,32,33] where CoO phase is formed at the end of charge process, rather than the completely reversible formation of Co_3O_4 phase. TEM images also indicate the partial loss of mesostructures during the discharge–charge process (Figure 3A–C), which is correlated well with the SAXS data.

In the case of meso-SnO_2 electrode (Figure 2C), the changes in the SAXS data are very different from those of the meso-TiO_2 and meso-Co_3O_4 electrodes. The position of SAXS peak slightly moves to lower angle until the discharge potential reaches to 1.2 V (region I), indicating the small expansion of mesoscopic cell volume (5.4%, Figure 4C). The d_{211} spacing

increases in the discharging range of 1.2−0.35 V, which consists of two steps: a rapid increase between 1.2−0.8 V (region II), and a moderate increase between 0.8−0.35 V (region III). Figure 4C indicates that the mesoscopic cell volumes increase up to 16.2% upon the lithiation until 5.2 mol of Li are stored in 1 mol of SnO_2 (region I, II and III in Figure 2D). The intensity of SAXS peak decreases dramatically in the region II and III, and the peak disappears completely below 0.35 V, where lithium ions are known to be stored by alloying reaction from this discharge potential.[15,34,35] The changes of mesostructural order and peak intensity have good correlation with our previous results concerning the Li-storage mechanism of the meso-SnO_2 electrode obtained by using synchrotron-based XRD and X-ray absorption spectroscopy analysis.[36] The SnO_2 crystallites are converted gradually into the amorphous nano-$LiSnO_2$ phase until the discharging voltage of ~0.6, where the conversion reaction is terminated and the alloying reaction starts, which are well-correlated with the intensity changes of SAXS peaks (Figure 2D). During the further lithiation (region IV), and moreover, delithiation process (region V), the SAXS peaks are not regenerated (Figure 2C). From these results, the highly ordered mesostructure of meso-SnO_2 electrode is fairly maintained during the conversion reaction, but completely collapsed by further reaction with lithium ions following the alloying reaction, which is not reconstructed to an ordered mesostructure even after dealloying process. The mesostructural change of meso-SnO_2 electrode can also be confirmed from the TEM images shown in Figure 3D,−F. There are no ordered mesostructures in the case of meso-SnO_2 after the lithiation (Figure 3E) and delithiation (Figure 3F).

CONCLUSIONS

In conclusion, the present *in operando* SAXS study clearly shows the nanostructural changes of the mesoporous electrode materials during discharge−charge process with respect to the amount of lithium reacted and maintainability of the mesoscopic pore structure during cycling, which are highly dependent on their Li-storage mechanisms. Moreover, the changes of mesoscopic cell volumes upon lithiation and delithiation also can be exactly measured, from which we can get direct evidence that proves the role of mesopores in the active materials to effectively accommodate the volume expansion of crystalline frameworks by the reaction with lithium. Such a precise *in operando* probing technique for pore dynamics of ordered porous materials can be also utilized to study nanostructural changes of the electrode materials in other electrochemical systems adopting porous materials, such as electrode of the fuel cells, supercapacitor and metal-air battery systems. We also believe that *in operando* investigation of dynamic changes in the mesoscale order will help us to deeply understand physical behaviors of lithium storage materials, thereby providing valuable guidance for designing innovative nanostructured materials for next generation energy storage system.

MATERIALS AND METHODS

Materials. Pluronic triblock copolymer P123 ($EO_{20}PO_{70}EO_{20}$, M_w = 5800, Aldrich), 1-buthanol (99.7 wt %, Aldrich), hydrochloric acid (HCl, 35 wt %, Aldrich), tetraethyl orthosilicate (TEOS, $SiC_8H_{20}O_4$, 98 wt %, Aldrich), titanium tetraethoxide ($Ti(OEt)_4$, Aldrich), cobalt nitrate hexahydrate ($Co(NO_3)_2 \cdot 6H_2O$, 97%, SAMCHUN), tin chloride dehydrate ($SnCl_2 \cdot 2H_2O$, 97%, JUNSEI), sodium hydroxide (NaOH, 98%, SAMCHUN), and hydrofluoric acid (HF, 49%, J. T. Baker) were used without further purification.

Preparation of Mesoporous Electrodes. In typical synthesis for mesoporous silica, KIT-6, with cubic *Ia3d* mesostructure,[23] 9.0 g of P123 was dissolved in a mixture of 325.5 g of distilled water, 9.0 g of 1-butanol, and 17.7 g of HCl. After the mixture stirred at 35 °C for 10 min, 19.4 g of TEOS was added to this solution under vigorous stirring. The resulting mixture was stirred for 24 h at 35 °C and subsequently kept in static condition at 100 °C for 24 h. The solid product was filtered, washed with distilled water several times and dried at 100 °C overnight. The obtained white power was washed with ethanol, dried at 80 °C for 12 h, and finally calcined under static air condition at 550 °C for 3 h to remove the structure-directing agent. Ordered mesoporous TiO_2, Co_3O_4 and SnO_2 materials (meso-TiO_2, meso-Co_3O_4, and meso-SnO_2, respectively) were synthesized through a nanoreplication method using the KIT-6 as the silica templates.[24−26] To synthesize the meso-TiO_2, 0.6 g of $Ti(OEt)_4$ and 30 mL of distilled water were first mixed to obtain a white precipitate. The precipitate was collected by centrifuge and decantation of supernatant, and dissolved by adding 0.8 g of HCl at room temperature. This clear TiO_2 precursor sol was impregnated into 1.0 g of the KIT-6 by simple incipient wetness method, and the composites were dried at 160 °C for 10 min. This impregnation−drying process is repeated several times and the samples were dried at 100 °C for 24 h. The material was heated under static air condition at 450 °C for 3 h. The silica template was removed by treating the composite material with an aqueous solution of NaOH several times. Finally, the obtained ordered mesoporous TiO_2 material was washed with distilled water several times, and dried at 80 °C for 24 h. The meso-Co_3O_4 and meso-SnO_2 materials were synthesized by a solvent-free infiltration method.[25,26] Typically, 0.9 g of $Co(NO_3)_2 \cdot 6H_2O$ and 1.0 g of $SnCl_2 \cdot 2H_2O$ were melted at 100 °C to liquid states, and poured into 1.0 g of the preheated KIT-6 at 80 °C, respectively. The composites were shaken vigorously for 1 h, and put in an oven at 80 °C for 24 h for spontaneous infiltration of metal precursors within the mesopores of KIT-6. The composite materials were heated under static air condition at 550 °C for 3 h and 700 °C for 3 h, respectively. The silica templates were removed by treating the resulting material with an aqueous solution of NaOH several times in the case of obtaining the meso-Co_3O_4, whereas an aqueous solution of HF (10 wt %) was used for the meso-SnO_2. Finally, the meso-Co_3O_4 and meso-SnO_2 materials, thus obtained, were washed with distilled water several times and dried at 80 °C for 24 h.

***In Operando* Synchrotron SAXS Characterization.** Schematic representation of *in operando* SAXS experimental setup is shown in Scheme 1. The *in operando* SAXS experiments were carried out at BL 9A U-SAXS beamline (PLS-II) using 2D CCD Detector (Rayonix SX165, USA) which was positioned 2 m away from the sample and measured scattering in the 2θ range of 0.3−2.5 (λ = 1.54 Å). The size of the focused beam was 300 μm in diameter and the energy of the beam was 11 keV. The 2D

patterns of the mesoporous samples during electrochemical cycling were recorded with a 1 s exposure time and 8 s detector readout time. The 2D patterns were scanned with the FIT2D software package to obtain the one-dimensional (1D) patterns in the form of the intensity *vs* 2θ.[37] The storage ring was operated at 3.0 GeV with a ring current of 300 mA.

Electrochemical Characterization. The electrodes were prepared by coating the slurries composed of ordered mesoporous powder (70 wt %), conductive agent (Super-P, 15 wt %) and polyamideimide (PAI, Solvay, 15 wt %) dissolved in *N*-methylpyrrolidone (NMP) on the Cu foil substrate. After coating, the electrodes were dried at 120 °C for 12 h under vacuum and pressed under a pressure of 200 kg cm^{-2}. The electrode assembled coin type half cell (CR2032) with Li metal as a counter and reference electrode in a dry room using a polyethylene (PE) membrane was used as a separator, 1 M $LiPF_6$ dissolved in a mixed solvent of ethylene carbonate (EC) and diethyl carbonate (DEC) (3:7, v/v; Panax Etec Co. Ltd.) as an electrolyte. Galvanostatic charge−discharge experiments were carried out with a WBCS-3000 battery cycler (Xeno Co.) at a constant current of 0.1 C (theoretical capacity of 335 mAh g^{-1} for meso-TiO_2, 890 mAh g^{-1} for meso-Co_3O_4, and 790 mAh g^{-1} for meso-SnO_2).

Material Characterization. Small- and wide-angle high resolution synchrotron X-ray powder diffraction measurements were collected at BL 9B HRPD beamline (PLS-II). The incident X-rays were vertically collimated using a mirror and monochromatized to a wavelength of 1.5475 Å using a double-crystal Si (111) monochromator. The detector comprises a set of six analyzer crystals and seven scintillation detectors. The storage ring was operated at 3.0 GeV with a ring current of 300 mA. N_2 sorption isotherms were collected using Micromeritics Tristar system at liquid N_2 temperature. The specific BET (Brunauer−Emmett−Teller) surface areas, and pore size distribution curves calculated by the BJH (Barrett−Joyner−Halenda) were obtained on the basis of the adsorption branches. Total pore volumes were measured at p/p_0 = 0.99. Scanning electron micrographs (SEM) were collected using LEO SUPRA 55 GENESIS 2000 instrument at an accelerating voltage of 15 kV. Transmission electron micrographs (TEM) are obtained using a G2 FE-TEM at an operating voltage of 200 kV.

Conflict of Interest: The authors declare no competing financial interest.

Acknowledgment. This work was supported by the Samsung Research Funding Center of Samsung Electronics (No. SRFC-MA1401-03 and SRFC-TA1403-03). This work was partially supported by the Human Resources Development program (No. 20124010203270) of the KETEP by the Korea government.

Supporting Information Available: XRD patterns, N_2 adsorption−desorption isotherms, SEM images, and TEM images (Figures S1−S5); surface areas and pore volumes of mesoporous electrodes (Table S1). This material is available free of charge *via* the Internet at http://pubs.acs.org.

REFERENCES AND NOTES

1. Poizot, P.; Laruelle, S.; Grugeon, S.; Dupont, L.; Tarascon, J.-M. Nano-Sized Transition-Metal Oxides as Negative-Electrode Materials for Lithium-Ion Batteries. *Nature* **2000**, *407*, 496–499.
2. Tarascon, J.-M.; Armand, M. Issues and Challenges Facing Rechargeable Lithium Batteries. *Nature* **2001**, *414*, 359–367.
3. Bruce, P. G.; Scrosati, B.; Tarascon, J.-M. Nanomaterials for Rechargeable Lithium Batteries. *Angew. Chem., Int. Ed.* **2008**, *47*, 2930–2946.
4. Idota, Y.; Kubota, T.; Matsufuji, A.; Maekawa, Y.; Miyasaka, T. Tin-Based Amorphous Oxide: A High-Capacity Lithium-Ion-Storage Material. *Science* **1997**, *276*, 1395–1397.
5. Shin, H. C.; Liu, M. Three-Dimensional Porous Copper-Tin Alloy Electrodes for Rechargeable Lithium Batteries. *Adv. Funct. Mater.* **2005**, *15*, 582–586.
6. Chan, C. K.; Peng, H.; Liu, G.; McIlwrath, K.; Zhang, X. F.; Huggins, R. A.; Cui, Y. High-Performance Lithium Battery Anodes Using Silicon Nanowires. *Nat. Nanotechnol.* **2008**, *3*, 31–35.
7. Jiang, J.; Li, Y.; Liu, J.; Huang, X.; Yuan, C.; Lou, X. W. Recent Advances in Metal Oxide-Based Electrode Architecture Design for Electrochemical Energy Storage. *Adv. Mater.* **2012**, *24*, 5166–5180.
8. Jamnik, J.; Maier, J. Nanocrystallinity Effects in Lithium Battery Materials: Aspects of Nano-Ionics. Part IV. *Phys. Chem. Chem. Phys.* **2003**, *5*, 5215–5220.
9. Guo, Y.-G.; Hu, J.-S; Wan, L.-J. Nanostructured Materials for Electrochemical Energy Conversion and Storage Devices. *Adv. Mater.* **2008**, *20*, 2878–2887.
10. Jiao, F.; Bruce, P. G. Mesoporous Crystalline β-MnO_2 - A Reversible Positive Electrode for Rechargeable Lithium Batteries. *Adv. Mater.* **2007**, *19*, 657–660.
11. Shi, Y.; Gou, B.; Corr, S. A.; Shi, Q.; Hu, Y.-S; Heier, K. R.; Chen, L.; Seshadri, R.; Stucky, G. D. Ordered Mesoporous Metallic MoO_2 Materials with Highly Reversible Lithium Storage Capacity. *Nano Lett.* **2009**, *9*, 4215–4220.
12. Shon, J. K.; Kim, H.; Kong, S. S.; Hwang, S. H.; Han, T. H.; Kim, J. M.; Pak, C.; Doo, S.; Chang, H. Nano-Propping Effect of Residual Silicas on Reversible Lithium Storage over Highly Ordered Mesoporous SnO_2 Materials. *J. Mater. Chem.* **2009**, *19*, 6727–6732.
13. Ren, Y.; Hardwick, L. J.; Bruce, P. G. Lithium Intercalation into Mesoporous Anatase with an Ordered 3D Pore Structure. *Angew. Chem.* **2010**, *122*, 2624–2628.
14. Wang, G.; Liu, H.; Liu, J.; Qiao, S.; Lu, G. M.; Munroe, P.; Ahn, H. Mesoporous $LiFePO_4$/C Nanocomposite Cathode Materials for High Power Lithium Ion Batteries with Superior Performance. *Adv. Mater.* **2010**, *22*, 4944–4948.
15. Huang, J. Y.; Zhong, L.; Wang, C. M.; Sullivan, J. P.; Xu, W.; Zhang, L. Q.; Mao, S. X.; Hudak, N. S.; Liu, X. H.; Subramanian, A.; et al. A. *In Situ* Observation of the Electrochemical Lithiation of a Single SnO_2 Nanowire Electrode. *Science* **2010**, *330*, 1515–1520.
16. Liu, X. H.; Huang, J. Y. *In Situ* TEM Electrochemistry of Anode Materials in Lithium Ion Batteries. *Energy Environ. Sci.* **2011**, *4*, 3844–3860.
17. Liu, X. H.; Liu, Y.; Kushima, A.; Zhang, S.; Zhu, T.; Li, J.; Huang, J. Y. *In Situ* TEM Experiments of Electrochemical Lithiation and Delithiation of Individual Nanostructures. *Adv. Energy Mater.* **2012**, *2*, 722–741.
18. Liu, X.; Wang, D.; Liu, G.; Srinivasan, V.; Liu, Z.; Hussain, Z.; Yang, W. Distinct Charge Dynamics in Battery Electrodes Revealed by *In Situ* and *Operando* Soft X-ray Spectroscopy. *Nat. Commun.* **2013**, *4*, 3568.
19. Wang, J.; Chen-Wiegart, Y.-C. K.; Wang, J. *In Operando* Tracking Phase Transformation Evolution of Lithium Iron Phosphate with Hard X-ray Microscopy. *Nat. Commun.* **2014**, *5*, 4570.
20. Sandí, G.; Joachin, H.; Kizilel, R.; Seifert, S.; Carrado, K. A. *In Situ* SAXS Studies of the Structural Changes of Polymer Nanocomposites Used in Battery Applications. *Chem. Mater.* **2003**, *15*, 838–843.
21. Tominaga, Y.; Endo, M. Ion-Conductive Properties of Polyether-Based Composite Electrolytes Filled with Mesoporous Silica, Alumina and Titania. *Electrochim. Acta* **2013**, *113*, 361–365.
22. Wiaderek, K. M.; Borkiewicz, O. J.; Pereira, N.; Ilavsky, J.; Amatucci, G. G.; Chupas, P. J.; Chapman, K. W. Mesoscale Effects in Electrochemical Conversion: Coupling of Chemistry to Atomic- and Nanoscale Structure in Iron-Based Electrodes. *J. Am. Chem. Soc.* **2014**, *136*, 6211–6214.
23. Kim, T.-W.; Kleitz, F.; Paul, B.; Ryoo, R. MCM-48-like Large Mesoporous Silicas with Tailored Pore Structure: Facile Synthesis Domain in a Ternary Triblock Copolymer-Butanol-Water System. *J. Am. Chem. Soc.* **2005**, *127*, 7601–7610.
24. Kim, S. S.; Lee, H. I.; Shon, J. K.; Hur, J. Y.; Kang, M. S.; Park, S. S.; Kong, S. S.; Yu, J. A.; Seo, M.; Li, D.; et al. Preparation of Highly Ordered Mesoporous TiO_2 Materials with Crystalline Framework from Different Mesostructured Silica Templates *via* Nanoreplication. *Chem. Lett.* **2008**, *37*, 140–141.

25. Shon, J. K.; Kong, S. S.; Kim, Y. S.; Lee, J.-H.; Park, W. K.; Park, S. C.; Kim, J. M. Solvent-Free Infiltration Method for Mesoporous SnO_2 Using Mesoporous Silica Templates. *Microporous Mesoporous Mater.* **2009**, *120*, 441–446.
26. Ahn, C.-I.; Koo, H. M.; Jin, M.; Kim, J. M.; Kim, T.; Suh, Y.-W.; Yoon, K. J.; Bae, J. W. Catalyst Deactivation by Carbon Formation during CO Hydrogenation to Hydrocarbons on Mesoporous Co_3O_4. *Microporous Mesoporous Mater.* **2014**, *188*, 196–202.
27. Solovyov, L. A.; Zaikovskii, V. I.; Shmakov, A. N.; Belousov, O. V.; Ryoo, R. Framework Characterization of Mesostructured Carbon CMK-1 by X-ray Powder Diffraction and Electron Microscopy. *J. Phys. Chem. B* **2002**, *106*, 12198–12202.
28. Tian, B.; Liu, X.; Solovyov, L. A.; Liu, Z.; Yang, H.; Zhang, Z.; Xie, S.; Zhang, F.; Tu, B.; Yu, C.; et al. Facile Synthesis and Characterization of Novel Mesoporous and Mesorelief Oxides with Gyroidal Structures. *J. Am. Chem. Soc.* **2004**, *126*, 865–875.
29. Hardwick, L. J.; Holzapfel, M.; Novák, P.; Dupont, L.; Baudrin, E. Electrochemical Lithium Insertion into Anatase-Type TiO_2: An *In Situ* Raman Microscopy Investigation. *Electrochim. Acta* **2007**, *52*, 5357–5367.
30. Lafont, U.; Carta, D.; Mountjoy, G.; Chadwick, A. V.; Kelder, E. M. *In Situ* Structural Changes upon Electrochemical Lithium Insertion in Nanosized Anatase TiO_2. *J. Phys. Chem. C* **2009**, *114*, 1372–1378.
31. Shin, J.-Y.; Samuelis, D.; Maier, J. Sustained Lithium-Storage Performance of Hierarchical, Nanoporous Anatase TiO_2 at High Rates: Emphasis on Interfacial Storage Phenomena. *Adv. Funct. Mater.* **2011**, *21*, 3464–3472.
32. Shaju, K. M.; Jiao, F.; Debart, A.; Bruce, P. G. Mesoporous and Nanowire Co_3O_4 as Negative Electrodes for Rechargeable Lithium Batteries. *Phys. Chem. Chem. Phys.* **2007**, *9*, 1837–1842.
33. Su, Q.; Zhang, J.; Wu, Y.; Du, G. Revealing the Electrochemical Conversion Mechanism of Porous Co_3O_4 Nanoplates in Lithium Ion Battery by *in Situ* Transmission Electron Microscopy. *Nano Energy* **2014**, *9*, 264–272.
34. Courtney, I. A.; Dahn, J. R. Electrochemical and *In Situ* X-ray Diffraction Studies of the Reaction of Lithium with Tin Oxide Composites. *J. Electrochem. Soc.* **1997**, *144*, 2045–2052.
35. Wang, C.-M.; Xu, W.; Liu, J.; Zhang, J.-G.; Saraf, L. V.; Arey, B. W.; Choi, D.; Yang, Z.-G.; Xiao, J.; Thevuthasan, S.; et al. *In Situ* Transmission Electron Microscopy Observation of Microstructure and Phase Evolution in a SnO_2 Nanowire during Lithium Intercalation. *Nano Lett.* **2011**, *11*, 1874–1880.
36. Kim, H.; Park, G. O.; Kim, Y.; Muhammad, S.; Yoo, J.; Balasubramanian, M.; Cho, Y.-H.; Kim, M.-G.; Lee, B.; Kang, K.; et al. New Insight into the Reaction Mechanism for Exceptional Capacity of Ordered Mesoporous SnO_2 Electrodes *via* Synchrotron-Based X-ray Analysis. *Chem. Mater.* **2014**, *26*, 6361–6370.
37. Hammersley. A. P. *FIT2D: An Introduction and Overview*; ESRF Internal Report, ESRF97HA02T **1997**.